Greenland and Canadian Arctic ice temperature profiles database

Anja Løkkegaard[1,2], Kenneth D. Mankoff[1,3,4], Christian Zdanowicz[5], Gary D. Clow[6], Martin P. Lüthi[7], Samuel Doyle[8], Henrik H. Thomsen[1], David Fisher[9], Joel Harper[10], Andy Aschwanden[11], Bo M. Vinther[12], Dorthe Dahl-Jensen[12], Harry Zekollari[13,14,15], Toby Meierbachtol[10], Ian McDowell[16], Neil Humphrey[17], Anne Solgaard[1], Nanna B. Karlsson[1], Shfaqat A. Khan[2], Benjamin Hills[18], Robert Law[19], Bryn Hubbard[8], Poul Christoffersen[19], Mylène Jacquemart[13,14], Julien Seguinot[20], Robert S. Fausto[1], and William T. Colgan[1]

[1]Geological Survey of Denmark and Greenland, Copenhagen, Denmark
[2]DTU Space, Technical University of Denmark, Denmark
[3]Autonomic Integra LLC, New York, NY, 10025 USA
[4]NASA Goddard Institute for Space Studies, New York, NY, 10025 USA
[5]Department of Earth Sciences, Uppsala University, Uppsala, Sweden
[6]Institute of Arctic and Alpine Research, University of Colorado Boulder, USA
[7]Geographical Institute, University of Zurich, 8052 Zurich, Switzerland
[8]Centre for Glaciology, Department of Geography and Earth Sciences, Aberystwyth University, Aberystwyth, SY23 3DB, UK
[9]Department of Earth and Environmental Sciences, University of Ottawa, Ottawa, Canada, K1N 6N5
[10]Department of Geosciences, University of Montana, Missoula, MT,59812, USA
[11]Arctic Region Supercomputing Center, University of Alaska Fairbanks, Fairbanks, AK, USA
[12]Centre for Ice and Climate, Niels Bohr Institute, University of Copenhagen, Copenhagen, Denmark, 2100
[13]Laboratory of Hydraulics, Hydrology and Glaciology (VAW), Birmensdorf, Switzerland
[14]ETH Zurich, Zurich, Switzerand; Swiss Federal Institute for Forest, Snow and Landscape Research (WSL)
[15]Laboratoire de Glaciologie, Université libre de Bruxelles, Brussels, Belgium
[16]Graduate Program of Hydrologic Sciences, University of Nevada, Reno, Reno, NV, USA
[17]Department of Geology and Geophysics, University of Wyoming, Laramie, WY, USA
[18]Department of Earth and Space Sciences, University of Washington, Seattle, WA, USA
[19]Scott Polar Research Institute, University of Cambridge, Cambridge, UK
[20]Department of Biology, University of Bergen and Bjerknes Centre for Climate Research, Bergen, Norway

Correspondence: Anja Løkkegaard (aloe@geus.dk)

Abstract. Here, we present a compilation of 95 ice temperature profiles from 85 boreholes from the Greenland Ice Sheet and peripheral ice caps, as well as local ice caps in the Canadian Arctic. Profiles from only 31 boreholes (36%) were previously available in open-access data repositories. The remaining 54 borehole profiles (64%) are being made digitally available here for the first time. These newly available profiles, which are associated with pre-2010 boreholes, have been submitted by community members or digitized from published graphics and/or data tables. All 95 profiles are now made available in both absolute (meters) and normalized (0 to 1 ice thickness) depth scales, and are accompanied by extensive metadata. This metadata includes a transparent description of data provenance. The ice temperature profiles span 70 years, with the earliest profile being from 1950 at Camp VI, West Greenland. To highlight the value of this database in evaluating ice flow simulations, we compare the ice temperature profiles from the Greenland Ice Sheet with an ice flow simulation by the Parallel Ice Sheet Model (PISM). We find a cold bias in modeled near-surface ice temperatures within the ablation area, a warm bias in modeled basal ice

temperatures at inland cold-bedded sites, and an apparent underestimation of deformational heating in high-strain settings. These biases provide process-level insight on simulated ice temperatures.

1 Introduction

With the tremendous social implications of sea-level change, the past decade has seen a proliferation of simulations of the current and future geometry and dynamics of the Greenland ice sheet (Bindschadler et al., 2013; Goelzer et al., 2020; Aschwanden et al., 2021). These present-day complex ice flow models build upon the legacy of simpler past thermo-mechanical models (Letréguilly et al., 1991; Huybrechts et al., 1991; Funk et al., 1994; Calov and Hutter, 1996). Due to the high sensitivity of ice viscosity to ice temperature, the thermal state of the ice sheet is a critical element of these simulations (Colgan et al., 2015). At present, however, the englacial temperature fields of even cutting-edge ice-sheet simulations remain largely unevaluated against observed temperatures (Aschwanden et al., 2019). While recent studies show potential for deriving internal ice temperatures from satellite or airborne data (Macelloni et al., 2019; Jezek et al., 2022), these techniques are not yet widely employed. There are consequently diverse opinions on Greenland's basal thermal state across the current generation of thermo-mechanical ice flow models (MacGregor et al., 2016).

Several different methods for measuring ice temperatures have been used on the Greenland Ice Sheet and in the Canadian Arctic. The methods include: borehole logging where a temperature sensor is moved up or down the borehole measuring either "continuously" as the probe moves or is stopped to measure at every depth known as "stop-and-go" (Johnsen et al., 1995; Clow, 2008); sensor strings (this term includes both digital and analog) where thermistors are frozen into the ice and ice temperatures are recorded at various depths at the same time (Iken et al., 1993; Ryser et al., 2014); and, fiber-optic distributed temperature sensing (DTS), where the ice temperature is measured near-continuously along the full cable length (Law et al., 2021). We summarize the methods and their advantages and disadvantages in Table 1.

Ice temperature profiles collected in Greenland and the Canadian Arctic have not been systematically compiled into a coherent database. In particular, many pre-1990 ice temperature profiles languished in undigitized reports or gray literature. This presented a clear motivation to assemble ice temperature measurements into a consistent and comprehensive community resource. Here, we describe our compilation of ice temperature profiles from Greenland and the Canadian Arctic into an open-access database with well-documented and uniform metadata for each entry. We include Canadian Arctic ice caps in our predominantly Greenland database, as these regions reside within the domain of some Greenland ice flow models (e.g. Tarasov and Peltier, 2004; Gowan et al., 2021).

The earliest temperature profile in our database is from 1950, when a 125 m profile was measured at Camp VI in West Greenland (Heuberger, 1954). Earlier temperature profiles may exist, and incorporating these profiles into the database is an ongoing process. We restrict our database to ice temperature profiles extending well below the depth of the seasonal temperature cycle. At cold, dry sites, this is often approximated to be 10 to 15 m below the surface (Cuffey and Paterson, 2010). Similar to a recent effort to compile surface mass balance observations into a readily accessible common framework (Machguth et al., 2016), we aim to create a community resource that facilitates comparisons between simulated and observed ice temperatures.

Here, we describe the format of the database as well as the sources of our ice temperature data and metadata. We also discuss
45 best practices for comparing observed ice temperatures with simulated ice temperatures from a 3-D thermo-mechanical model.
Finally, we make an appeal to community colleagues to continually update this dataset, providing instructions for them to do
so.

Table 1. Advantages and disadvantages of the main methods for measuring deep ice temperatures. This compilation ignores the absolute
accuracy of the ice temperature sensor, which can vary greatly within any one method type.

Method	Advantages	Disadvantages
Borehole logger	• recoverable and reusable, leaves the borehole empty • continuous logging is possible over entire borehole depth	• some require 'stop-and-go' measurements to equilibrate at each measurement depth • logger depth uncertainty between individual measurement depths • measurements require on-site presence, and thus unattended time series, are not possible
Thermistor string	• relatively cheap instruments and data logger at the ice surface • unattended ice profile measurements through time are possible • voltage-based measurements are a relatively simple and established technology	• single deployment, cable generally not recovered when frozen in borehole • cable resistance correction must be calculated for large ice depths • number of measurements with depth limited as each thermistor requires a separate cable core
Digital sensor string	• relatively cheap instruments and data logger at the ice surface • unattended ice profile measurements through time are possible • large number of sensors with depth possible with common cable and data transfer protocols • measurement is not affected by cable resistance or capacitance effects	• single deployment, cable generally not recovered when frozen in borehole • detection of temperature change limited by resolution • heat dissipation from electronics can affect measurements
Fiber-optic distributed sensing string	• near-continuous vertical ice temperature profile • unattended ice profile measurements through time are possible • no inter-sensor uncertainty at different depths	• single deployment, cable generally not recovered when frozen in borehole • sensitive and expensive data logger at ice surface • relatively expensive compared to thermistor and digital sensor strings

2   Temperature Data

The temperature database currently comprises a total of 95 temperature profiles. In two instances the same borehole was logged twice at different times (Thomsen et al., 1991). Other boreholes which have been logged more than once also include GISP2-D, GISP2-G, NGRIP-2, NGRIP-S2, NEEM-D, however, these are currently not included in the database. The database also contains partial temperature profiles, which are considered to make up one profile. This is the case for the two sites FOXX6 and GULL1 (Ryser et al., 2014). Furthermore, five partial profiles at one site (Lüthi et al., 2002) all situated less than 25 m from one another were also regarded as one borehole. This means that the 95 temperature profiles in the database are considered to originate from 85 unique boreholes.

See Figure 1 for an overview of the drill site locations, and the database for the complete list of borehole IDs. Borehole IDs denote the general location of the borehole, project-specific borehole IDs if multiple boreholes exist at that location, and the year of the measurement. Borehole temperature records were entered into the database in two different formats: A) tabulated original measurements, provided either by community members or obtained from historical reports, or B) published graphics of measured temperature profiles digitized using the publicly available digitization tool WebPlotDigitizer (https://automeris.io/WebPlotDigitizer; Last Access 3 March 2022; Rohatgi (2021)).

Overall, 71 of the 95 profiles were available as tabulated temperature measurements (Heuberger, 1954; Classen, 1977; Stauffer and Oeschger, 1979; Clarke et al., 1987; Thomsen et al., 1991; Iken et al., 1993; Hansson, 1994; Cuffey et al., 1995; Thomsen et al., 1996; Cuffey and Clow, 1997; Dahl-Jensen et al., 1998; Fischer et al., 1998; Lüthi et al., 2002; Kinnard et al., 2006; Buchardt and Dahl-Jensen, 2007; Kinnard et al., 2008; Lemark and Dahl-Jensen, 2010; Rasmussen et al., 2013; Ryser et al., 2014; Harrington et al., 2015; Hills et al., 2017; Zekollari et al., 2017; Doyle et al., 2018b; Seguinot et al., 2020; Hubbard et al., 2021a; Harper and Meierbachtol, 2021; Law et al., 2021). The remaining 24 profiles were digitized from figures (Hansen and Landauer, 1958; Davis, 1967; Paterson, 1968; Classen, 1977; Paterson et al., 1977; Colbeck and Gow, 1979; Gundestrup and Hansen, 1984; Blatter and Kappenberger, 1988; Gundestrup et al., 1993).

Here, we describe both the initial Dataverse database release (Mankoff et al., 2022) and the GitHub living repository (Mankoff, 2022). The Dataverse database (Mankoff et al., 2022) contains four curated files: two comma-separated value (CSV) files with temperature and depth-normalized temperature at each site, a KML file of borehole locations, and a metadata file. The GitHub living repository (Mankoff, 2022) is where raw data is collected, curated, and documented in order to create the final data. The repository is termed living, because it is also the entry point for new data into future database versions.

GitHub living repository (Mankoff, 2022) consists of high-level post-processed CSV files ready for use, and low-level folders with original sources and notes for each temperature profile. The CSV files include two data files combining all profiles, one file with depth in units of meters with a step size of 1 m, and another file with normalized depth as 0-1 with a step size of 0.01. This standardization of the profiles from coarse discrete measurements to uniformly finely spaced values was done by interpolating between points, using cubic spline interpolation with no overshoot. A third CSV file combines all metadata for each profile and, finally, a GIS file (format KML) provides borehole locations. Folders also contain a file named "data.csv"
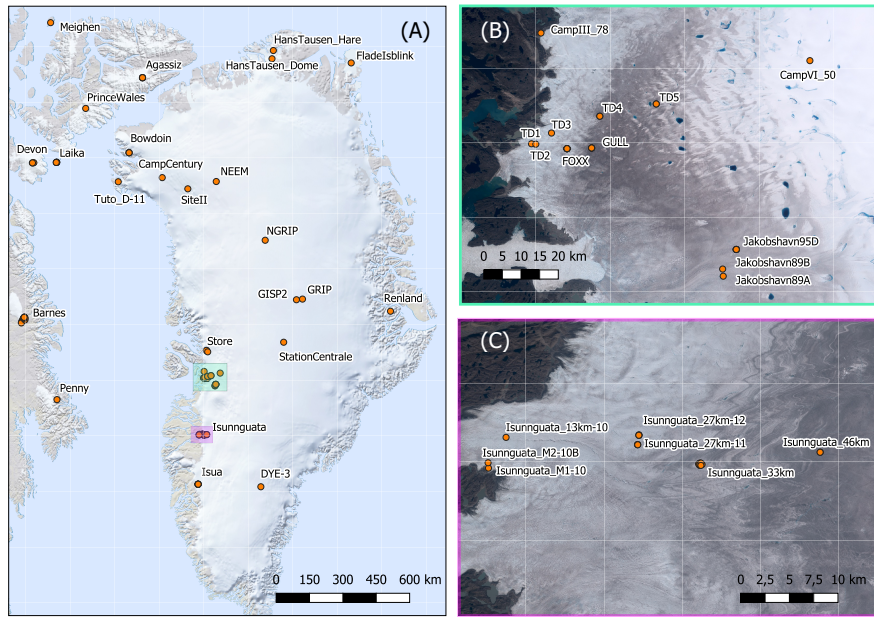
Figure 1. (A): Overview of the drill site locations of temperature profiles contained in the database (plot created using QGreenland, Moon et al. (2021)). Note, locations where several drill sites exist close to each other, only the common name is shown, e.g. Agassiz. The green and purple box indicates regions where numerous profiles have been drilled. **(B)**: Zoomed view of the region near Jakobshavn glacier. **(C)**: Zoomed view of the region near Isunnguata Sermia glacier. Panels **(B)** and **(C)** show positions plotted on top of Sentinel-2 multispectral satellite imagery, 10 m resolution from 2019 (MacGregor et al., 2020). All maps are displayed in EPSG: 3413 polar stereographic projection, with the Easting and Northing given in meters.

that is the original data at the original depth resolution, a README.org file with any relevant notes, including "cleaned" email correspondence when personal communications were involved in recovering the data, or other files detailing data acquisition.

Where ice temperature profiles are derived from a graphic (Barnes_(B4,D4)_1974, Barnes_T0(975_1976, 91_1977, 81_1978, 61_1977, 20_1979), Camp Century, Devon72, Devon73, DYE-3, Isua_10-14, Laika_75a-75e, Meighen67, SiteII, Tuto_D-11), the graphic is included in the folder. These folders also include a .tar or JSON file, which can be opened in WebPlotDigitizer, that contains the digitized profile and shows the digitization method. Graphical temperature data was digitized in the following way: the figure was loaded into WebPlotDigitizer as an xy-plot. The axis of the figure was then calibrated by defining two points on each axis, with these definition points preferably being as far away from each other as possible. The program has two options for digitizing, "manual" or "automatic" extraction, and typically a combination of both methods was used. Using the automatic mode, profiles were defined by creating a mask, and an automatic extraction was used to produce an initial set of points. The manual mode was then used to adjust these points where necessary to fine tune visual match to the graphic. For figures that contained both in-situ temperature points and a fitted temperature line, only the points were detected using WebPlotDigitizer's "blob detector" automatic algorithm.

Digitizing data from graphics can introduce non-trivial digitization uncertainty associated with potentially improper alignment of the defining axes (systematic uncertainty) and/or improper alignment of the data points (random uncertainty). The magnitude of this digitization uncertainty is proportional to the sizes of the graphic and data range, which vary from profile to profile. To highlight the potential importance of digitization uncertainty, we propagate the uncertainty associated with a ±2 pixel error in each of the axes defining points for both temperature and depth in the digitized profiles with the thinnest ice (Tuto_D-11; 48 m) and the thickest ice (DYE-3; 2038 m). The Tuto_D-11 graphic (Davis, 1967)(Figure 2A) is 1,000 pixels tall and spans 47.5 m, which yields a ±2 pixel depth uncertainty of ±0.15 m. The Tuto_D-11 graphic is 600 pixels wide and spans 32 °C, which yields a ±2 pixel temperature uncertainty of ±0.1 °C. In comparison, the DYE-3 graphic (Gundestrup and Hansen, 1984)(Figure 2B) is 1200 pixels tall, spans 2200 m and yields a ±2 pixel depth uncertainty of ±3.6 m. The DYE-3 graphic, 900 pixels wide, spans 8 °C and yields a ±2 pixel temperature uncertainty of ±0.02 °C. These end-member scenarios highlight how digitization uncertainty varies from graphic to graphic.
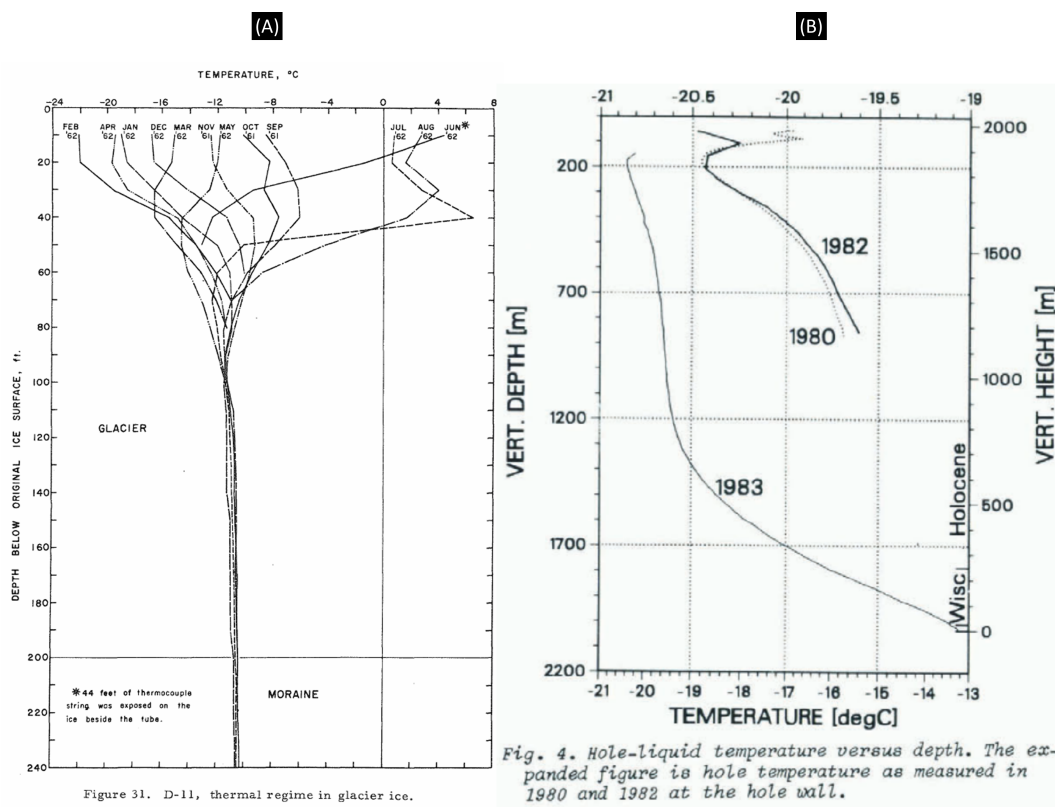
Figure 2. (**A**): Graphic from which the Tuto_D-11 profile is digitized (Davis, 1967). This figure is reproduced from a US Government publication. (**B**): Graphic from which the DYE-3 profile is digitized (Gundestrup and Hansen, 1984). This figure is reproduced with permission from the International Glaciology Society.

105 All ice temperature profiles – from both digitized and tabulated sources – were standardized by interpolating between points, using cubic spline interpolation with no overshoot, in order to resolve the two common depth scales: the absolute depth scale at 1 m vertical resolution (Figure 3A, C, E) and the normalized depth scale at non-dimensional 0.01 vertical resolution (Figure 3B, D, F). The latter allows easy comparison between sites of different ice thicknesses, and is useful in overcoming slight differences in ice thickness when comparing observed and modeled temperature profiles. The normalized

110 depth scale temperature file is named "temperature_dnorm.csv". The absolute depth scale temperature file, which is expressed as temperature with depth from the surface, is named "temperature.csv". In each file, 'NaN' means that no temperature data is available at the given depth, and in the absolute depth file '-999' refers to an elevation below bedrock. Ice thicknesses vary significantly across the database profiles, from 3085 m at NGRIP to 48 m at Tuto_D-11, so the number of -999 below-bed null-values varies between sites. This is because the temperature vector length is constant across the database entries, but the

115 ice thickness varies across database entries.

3 Metadata

The database includes additional supplementary information. For each borehole, this information is stored in the file "meta.csv", which contains a total of 18 metadata fields (Table 2). Every measurement entry in the database is labeled with a unique **borehole ID**, and a non-unique alternative more descriptive **place name**. This alternative place name was deemed useful as, in

120 some cases, ice temperature profiles have been measured over different campaigns by different people who have used different nomenclature for the same sites. Furthermore, borehole ID's are generally defined by either the group carrying out the measurements or by the site of the measurement. These borehole IDs are somewhat inconsistent, however, based on the differing conventions used by previously published studies.

Whenever specific locations are available, that of each ice temperature borehole is provided in degrees east **longitude**

125 and degrees north **latitude**. In some cases, locations have been shown in figures in accompanying literature, from which approximate locations were georeferenced. In addition to the position of the borehole, three further sets of information are provided relating to geographic setting. **Site type** describes whether the profile samples the Greenland Ice Sheet or a local ice cap. **Geographic location**, which provides a more descriptive general location of borehole sites using recognized regional geographic names. Lastly, the **source** of the **location** information.

130 The local **ice thickness** at the borehole location is provided in meters, along with the **ice thickness source**. When the original literature does not report local ice thickness, an estimate is provided using BedMachine v3 (Morlighem et al., 2017). In these instances, the ice thickness is useful to determine the fraction of the ice depth, from the surface to the bed, covered by the given temperature profile, given as the percentage **coverage** in another field. Also listed are the depth in meters from the surface of the ice sheet to the uppermost temperature measurement of a given profile (**depth of top**), and the lowermost temperature

135 measurement (**depth of bottom**).

For each profile, **data source**, describes the source of the temperature data, including links to open-access data repositories used by authors to share the original data, and the **science source**, which lists any original scientific publication that describes
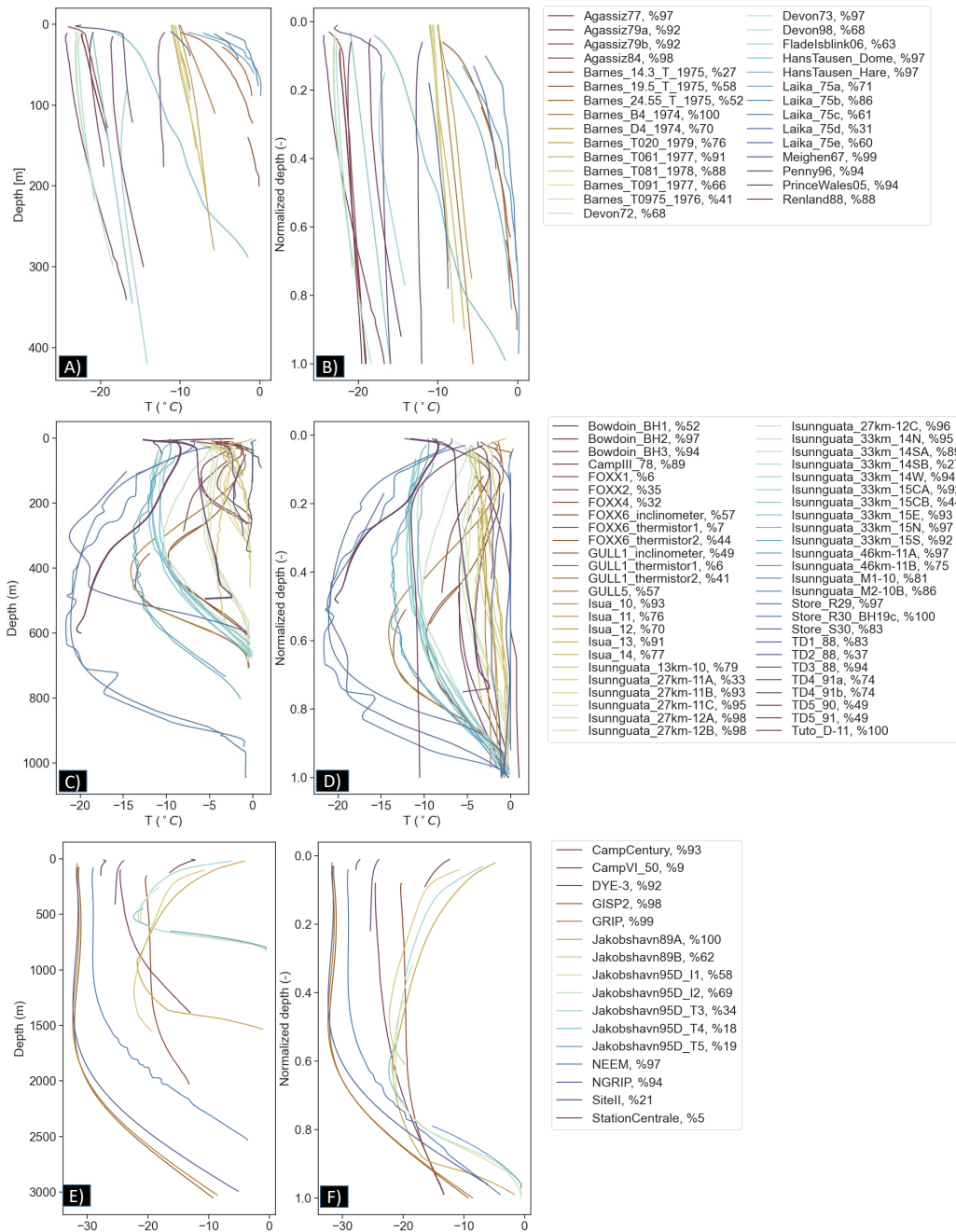
Figure 3. Overview of all ice temperature profiles in the database expressed in both absolute depth (**A**),(**C**),(**E**) and normalized depth (**B**),(**D**),(**F**). For visibility, the profiles are divided into local ice caps (**A**)-(**B**), marginal ice-sheet sites (**C**)-(**D**), and inland ice-sheet sites (**E**)-(**F**). The local ice thickness coverage of each individual profile is given as a percentage.

or mentions the temperature data. The related **DOI** for both the data and science source categories are also reported when available. **Date** describes the common era year when the temperature profile was measured. In the best cases, this includes the

140 month and day a given profile was measured. Finally, a field for additional **notes** is included, presenting any further information (relating to, for example, temperature, thickness or location) that does not fit into the above categories.

Despite the best efforts of our community, there are some missing metadata fields in the database, denoted by a question mark. The database is being continually updated. Any additional information, such as missing, updated or new temperature data, may be added to the database by contacting the author team here, or opening a GitHub issue at https://github.

145 com/GEUS-Glaciology-and-Climate/greenland_ice_borehole_temperature_profiles/issues (Last Access 1 March 2022). We use GitHub issues to resolve and identify and clarify problems in the ice temperature datasets, and we also welcome any new or missing data into the database via GitHub issues.

Table 2. Description of the database metadata structure. The fields are bolded where they appear in the text.

Field	Description
Borehole ID (text)	Unique name for each measured profile.
Place name (text)	Non-unique name for the site at which the profile is located.
Geographic location (text)	General region within which the site is located.
Site type (text)	Whether the profile samples the 'ice sheet' or a 'local ice cap',
Date (YYYY-MM-DD)	Date of the temperature profile measurement. Nearest year if specific date not available.
Longitude (°E)	Longitude of the borehole.
Latitude (°N)	Latitude of the borehole.
Location source (text)	Source of the borehole coordinates.
Ice thickness (m)	Ice thickness measured or estimated at the borehole.
Ice thickness source (text)	Source of the ice thickness, citation information and link to original open-access data repository used.
Depth of top measurement (m)	Depth to the uppermost temperature measurement in the borehole.
Depth of bottom measurement (m)	Depth to the lowermost temperature measurement in the borehole.
Coverage (%)	Fraction of the ice depth, from the surface to bed, covered by the ice temperature measurements.
Data source (text)	Source of the temperature data.
Data DOI (text)	DOI of the temperature data (if available).
Science source (text)	Scientific publication about the temperature data (if available).
Science DOI (text)	DOI of the science reference (if available).
General note (text)	General notes associated with any given temperature profile.

4   Data Summary

Of the 95 deep ice temperature profiles making up the database, 70 originate from Greenland and 25 from the Canadian Arctic

150   Figure (1). Of the 70 profiles from Greenland, 66 are from the ice sheet, and four are from peripheral glaciers and ice caps. All 29 peripheral glaciers and ice cap temperature profiles are plotted together in Figure 3A, B. The peripheral glacier and ice cap profiles are relatively shallow: the deepest reaches 420 m at a site where ice thickness is estimated to be 520 m. Profiles from the ice sheet are divided into 50 marginal profiles (Figure 3C, D) and 16 inland profiles (Figure 3E, F), according to proximity

to the main flow divide. The profile at GISP2, reaching bedrock at depth 3053 m and with a local ice thickness coverage of
155 98%, is the deepest measurement in the database. Overall, 9 of the 95 profiles reach depths >1000 m.

The inland profiles also exhibit the coldest temperatures, with temperatures reaching a minimum of around -32°C halfway down the profile at normalized depth 0.48. Thirty-four of the database's 95 profiles are from locations characterized as "cold-bedded", where the ice appears to be frozen to the bedrock. This characterization is assigned based on the observed bottom values of the profile. At some sites we cannot speculate on the basal thermal state based on temperature observation alone.
160 Eight of these "cold-bedded" profiles extend to >95% of local ice thickness (i.e., database coverage >95%). This contrasts with 56 "warm-bedded" sites where the ice at the bed is at pressure melting point. 15 of these warm-bedded profiles extend to >95% of local ice thickness. The basal thermal state of the three sites CampIII_78, CampVI_50, and SiteII, cannot be characterized, as these boreholes covered less than 25% of the local ice thickness. Overall, 39 of the 95 profiles have a depth coverage >90%.

The temporal distribution of the profiles shows how the number of available ice temperature measurements has increased
165 over time (Figure 4). The temperature profiles span a period of 70 years. This implies that the shallow measurement points cannot necessarily be expected to reflect current ice temperatures. Arctic air temperatures have warmed markedly during the past seven decades. The response time for deep ice temperature variations, however, is usually much longer than 70 years (Cuffey and Paterson, 2010). For example, at a low-accumulation site in the ice-sheet interior, a surface air temperature signal from c. 50 years ago can likely influence present-day ice temperatures at >50 m below the ice-sheet surface (Muto et al., 2011;
170 Karlsson et al., 2020).
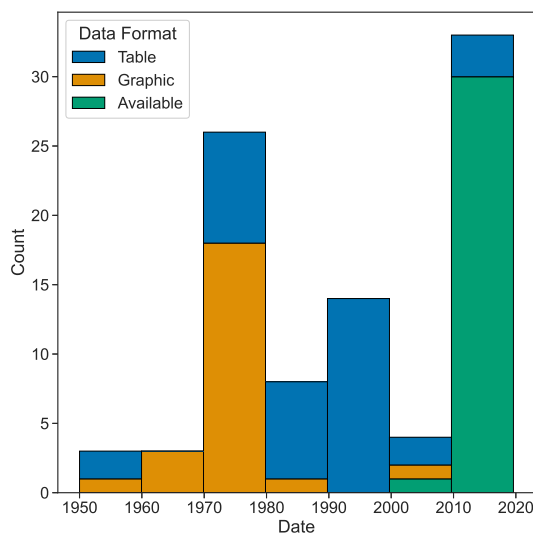
Figure 4. Histogram showing the temporal distribution of temperature profile measurements, color coded based on the format the original data was available as. The profiles entered into the database were available as: digitized graphic (orange), digitized table (blue), or is already published and digitally available (green).

The majority of the ice temperature profiles presented here have not been previously available in digital format. Profiles from only 31 boreholes (c. 36% of the database) have been previously published in open-access data repositories (Ryser et al., 2014; Harper, 2017; Doyle et al., 2018a; Seguinot et al., 2020; Hubbard et al., 2021b; Law et al., 2021). The public availability of these profiles highlights the laudable open-science trend in the natural sciences. While we present derived products of these profiles, we provide links to the open-access repositories where data were originally deposited and encourage database users to recognize and cite these previous data repository sources where applicable. Profiles from 54 boreholes (c. 64% of the database) are made digitally available here for the first time. This includes profiles from 24 boreholes that were provided as tabulated data by community members, profiles from 24 boreholes that were digitized from previously published graphics, and 6 that were previously available as published tables.

5 Sources of Uncertainty

Borehole ice temperature measurements are associated with at least three main sources of uncertainty: measurement uncertainty, depth uncertainty and disturbance uncertainty. There are other sources of uncertainty that we do not consider here, such as self-heating of the sensor, sensor calibration and leakage path to name a few (e.g. Clow et al., 1996; Clow, 2008). Measurement uncertainty reflects the accuracy with which a temperature sensor can measure ice temperature. This uncertainty is influenced by both the design and calibration of the temperature sensor. It is reasonable to suggest that temperature sensor accuracy has improved by at least an order of magnitude from 1950 to today, from perhaps ± 0.1 °C in the 1950s to an effective limit of better than ± 0.01 °C today. This trend primarily reflects improvements in the down-borehole technology deployed in glaciological applications, not the absolute accuracy of temperature sensors available for public purchase.

The issue of depth uncertainty is greatest in ice temperature profiles measured by manually-deployed loggers. Manual loggers can have a characteristic depth uncertainty of $\pm 1\%$. By contrast, automated winch-deployed loggers typically use rotary encoders to measure logger depth with an uncertainty better than $\pm 0.01\%$. For example the GISP2 borehole has a drill depth of 3053 m but a logger depth of only 3050 m, which represents a discrepancy of $\pm 0.001\%$ (Cuffey et al., 1995). At deep interior sites, the temperature gradient in the lower part of the ice column is typically of the order of 0.02 K/m (cf. Figure 3E,F). At fast moving sites, the temperature gradient may be even larger (cf. Figure 3C,D) thus increasing the temperature uncertainty associated with depth uncertainty. At shallow sites, temperature gradients are typically small (cf. Figure 3A,B) making the depth uncertainty negligible. For example, at Camp Century the temperature profile was likely measured with a depth accuracy higher than $\pm 0.1\%$. With a measured basal temperature gradient of 17.5 °C/km, this is equivalent to an ice temperature uncertainty of ± 0.025 °C at the maximum borehole depth of 1388 m. There are, however, some site settings – especially when using manually-deployed loggers, logging non-vertical boreholes, or measuring extreme basal temperature gradients – in which depth uncertainty can actually play a larger role in ice temperature uncertainty than temperature sensor accuracy.

Disturbance uncertainty, which is associated with ice temperatures equilibrating after drilling, is a third source of measurement uncertainty. In boreholes filled with drilling fluid, disturbance uncertainty can include the development of convection cells

within the equilibrating drilling fluid. Convection cells are expected to occur when the temperature gradient in the ice exceeds a critical value dependent on the sum of a lapse rate term and the critical potential-temperature gradient (Clow, 2014). The size and strength of convection cells is a poorly defined function of drilling fluid density, borehole diameter and ice temperature gradient. In the Agassiz77 borehole, slight thermal instabilities in the drilling fluid produced temperature offsets of ±0.05 °C around the mean ice temperature gradient. In the NEEM 2011 profile, however, the convection cells between 1500 and 2000 m depth reach c. 50 m vertical length scale and produce ±0.5 °C offsets around the mean ice temperature gradient (Figure 5). The GISP-D temperature log (not presented here) also shows pronounced laminar convection cells between 1600 and 2000 m depth (Clow et al., 1996).
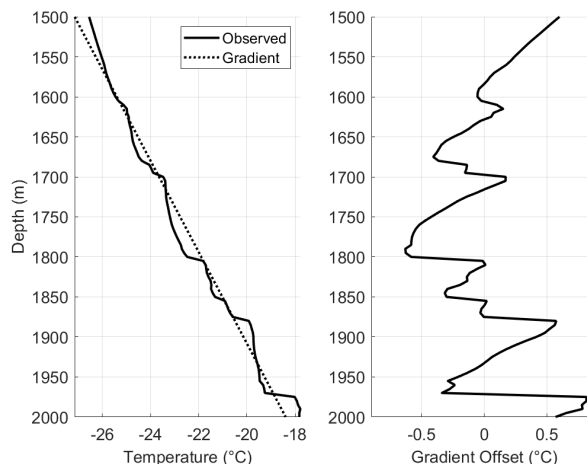
Figure 5. Offsets from the mean ice temperature gradient highlight the influence of large (c. 50 m) convection cells forming in the borehole fluid in a deep section of the NEEM ice temperature profile measured in 2011. These borehole fluid convection cells contribute to disturbance uncertainty associated with an equilibrating borehole temperature profile when the borehole logging technique is used. This uncertainty is avoided when sensors or cables are frozen into the ice in other measurement techniques.

Given the ultra-low density of air, air-filled boreholes cannot support analogous convection cells. The disturbance uncertainty associated with convection cells is accordingly negligible in air-filled boreholes. However, temperature disturbances due to changes in atmospheric pressure have been observed in air-filled bore holes in Antarctica. This effect is largest in the top 20 m of the borehole, just below the ice surface, with magnitudes on the order of up to ±0.003 °C (Clow et al., 1996). In water-filled boreholes, such as those created by hot-water drilling, disturbance uncertainty is associated with the sensible heat released from hot drilling water and the latent heat released by borehole refreezing. This thermal disturbance of hot-water drilling often requires many months to fully dissipate, as the latent energy released by the refreezing borehole warms surrounding ice. Empirical cooling curves of temperature measurements collected multiple times post drilling can usually constrain this thermal disturbance effect to better than ±0.1°C (Humphrey and Echelmeyer, 1990; Ryser et al., 2014; McDowell et al., 2021). Mechanically drilled ice-core holes also experience thermal disturbance, resulting primarily from the sensible heat carried into

the hole by the drill fluid. The associated disturbance uncertainty is, however, much smaller than for hot-water drilled holes (Clow et al., 2015). The temperature disturbance caused by mechanical drilling with fluid-filled boreholes dissipates to the level of precision within five days (Zagorodnov et al., 2012).

225 The total measurement uncertainty varies substantially between profiles in this database. Generally, these sources of uncertainty can be viewed as independent from each other, and therefore summed to estimate the total measurement uncertainty for a given ice temperature profile. Assessing this total measurement uncertainty is most critical for studies focused on absolute temperature, for example, when re-measuring present day ice temperatures to compare with past ice temperatures at a specific site. We provide guidance for assessing total measurement uncertainty by contrasting the uncertainty budgets of an older

230 (Tuto_D-11; 1962) and younger (Store_R30; 2019) ice temperature profile (Table 3). The Tuto_D-11 ice temperature profile is from an air-filled borehole in which ice temperature was measured with c. 60-year-old sensor technology using a manually-deployed logger. The Tuto_D-11 data also includes an additional graphical digitization uncertainty described in Section 2. The Store_R30 ice temperature profile was measured using a fiber-optic string frozen into a hot-water drilled borehole that was continuously monitored to establish empirical cooling curves. The contrasting uncertainty budgets of these two boreholes (see

235 Table 3) highlights the value of consulting the original science source publication for site-specific uncertainty assessments.

Table 3. Contrasting total measurement uncertainty budgets for the Tuto_D-11 and Store_R30 ice temperature profiles. The conversion of depth uncertainty into a temperature uncertainty is done assuming a characteristic temperature geothermal gradient of 20 °C/km. Here negligible means the uncertainty is <0.01 °C.

Uncertainty Source	Tuto_D-11 (1962)	Store_R30 (2019)
Measurement	±0.1 °C	±0.01 °C
Depth	±0.01 °C	negligible
Disturbance	negligible	±0.05 °C
Digitization	±0.1 °C	negligible
Total Uncertainty	**±0.21 °C**	**±0.06 °C**

6 Comparison with Simulated Ice Temperatures

Numerical ice flow models are critical tools for projecting the future sea-level rise contribution from the Greenland ice sheet. While the simulated initial states are typically evaluated against observed ice-sheet form (i.e. thickness) and flow (i.e. velocity), the relative paucity of ice temperature data means that they are typically not evaluated against observed ice-sheet thermal state

240 (Goelzer et al., 2020). Given the sensitivity of ice viscosity to ice temperature, biases in the thermal state of ice-sheet simulations likely contribute to biases between simulated and observed recent Greenland ice loss (Goelzer et al., 2017; Aschwanden et al., 2019; Law et al., 2021). Identifying and addressing these biases in thermal state is critical for improving projections of

Greenland ice loss (Aschwanden et al., 2021). To help shape best practice for using the database that we present, we describe an approach for evaluating a contemporary ice-sheet simulation against all observed Greenland deep ice temperature observations.

245   Several process-level studies of potential heat sources have been performed, which compare individual observed temperature profiles from local areas with temperature profiles modeled by a thermal, or themo-mechanical, ice flow model (Iken et al., 1993; Lüthi et al., 2002; Harrington et al., 2015; Lüthi et al., 2015; Meierbachtol et al., 2015; McDowell et al., 2021; Law et al., 2021; Maguire et al., 2021). Although these studies featured different local areas, the comparisons generally showed that models tend to underestimate englacial temperatures, and thus need to incorporate additional heat sources in order to

250 reproduce observed ice temperature profiles. Suggested additional heat sources include cryo-hydrological warming, which transfers latent heat when surface melt water flows through englacial pathways and re-freezes, as well as deformational heating and basal water heat flux (Funk et al., 1994; Wohlleben et al., 2009; Phillips et al., 2013; Lüthi et al., 2015; Zekollari et al., 2017; Karlsson et al., 2020). Modelled ice temperatures are likely also influenced by the choice of geothermal heat flow map, however, there is a diversity of opinion regarding the magnitude and spatial distribution of geothermal heat flow beneath the

255 ice sheet (Rezvanbehbahani et al., 2017; Colgan et al., 2022).

    The contemporary thermo-mechanical ice-sheet simulation we adopt is the Parallel Ice Sheet Model (PISM; Bueler and Brown (2009)) simulation of Aschwanden et al. (2016). This simulation represents the form, flow and thermal state of the Greenland ice sheet in c. 1990, following a 125 ky paleo-climatic spin-up, followed by another 2 ky of transient equilibrium with mass-flux adjustment forcing to minimize misfit against observed ice-sheet thickness and extent. This ice-sheet simulation

260 has a horizontal resolution of 900 m and a vertical resolution of 20 m. The geothermal heat flow map by Shapiro and Ritzwoller (Shapiro and Ritzwoller, 2004), variable in space but not time, was used as a basal thermal boundary condition. PISM uses an enthalpy scheme for the conservation of energy calculation, in order to accommodate heat transfer in both freezing and temperate ice (Aschwanden et al., 2012). While the spin-up is meant to approximate the Greenland Ice Sheet at a specific time slice (c. 1990), we are comparing this simulated thermal state with temperature profiles observed over a 70-year time span.

265 Shallow profiles located close to the margin can experience significant changes in ice thickness and temperature on this time scale.

    At locations of observed temperature profiles, modeled vertical temperature profiles were extracted from the PISM simulation based on the nearest neighbor grid point. Only temperature profiles from the Greenland Ice Sheet were included in this analysis. The PISM vertical temperature profiles were transformed from height above bed, to normalized depth below surface,

270 and linearly interpolated to the vertical resolution of the normalized depth field of the database. Further, at a few drill site locations, the modeled ice was too thin, and did not have enough vertical grid points to interpolate the modeled temperatures to a proper normalized depth axis. It was therefore necessary to exclude profiles from the analysis where the simulated ice thickness was less than 5 vertical grid points (50 m). Additionally, in cases of temporally-repeated observed profiles, only the most recent measurement was included in this analysis see Table 4.

275   Out of the 95 temperature profiles from the temperature database, 66 were ultimately suitable for inclusion in this comparative analysis of observed and modeled ice temperatures. The observed temperature profiles were divided based on three characteristic regimes. First, whether profiles were located in the accumulation area (16 profiles) or ablation area (38 profiles).

Secondly, whether the basal thermal state of profiles were considered warm-bedded (44 profiles) or cold-bedded (9 profiles). Finally, whether profiles were located in high-strain regions (10 profiles) or low-strain regions (46 profiles). The surface mass balance regime is determined by whether the borehole is located below the snow line, in the ablation area, or above snow line, in the accumulation area, in contemporary satellite imagery (Figure 1). The basal thermal state regime is based on whether the ice-bed interface is measured to be below the pressure-melting-point temperature (i.e. cold-bedded), or not (i.e. warm-bedded). In instances where the borehole does not reach the bed, we extrapolate the basal thermal state where reasonable (i.e. FladeIsblink06 is likely cold-bedded), or we list basal thermal state as "unknown" where the extrapolation distance seems unreasonable (i.e. CampVI_50 is unknown). Finally, ice dynamic regime is classified as high strain when the ice flow is channelized, and low strain when sites are located in sheet- or divide-flow. Figure 6 shows the observed temperature profiles for each of the three regimes.

Table 4. Overview of the number of profiles in the three regimes before and after excluding profiles not usable for the model comparison analysis.

	Surface mass balance regime	Basal thermal state regime	Ice dynamic regime
Initial Number of profiles	16 accumulation 48 ablation 2 unknown	10 cold bedded 53 warm bedded 3 unknown	13 high strain rate 53 low strain rate
Total	66	66	66
Number of profiles after exclusions	16 accumulation 40 ablation	6 cold bedded 49 warm bedded	13 high strain rate 44 low strain rate
Total	56	55	57
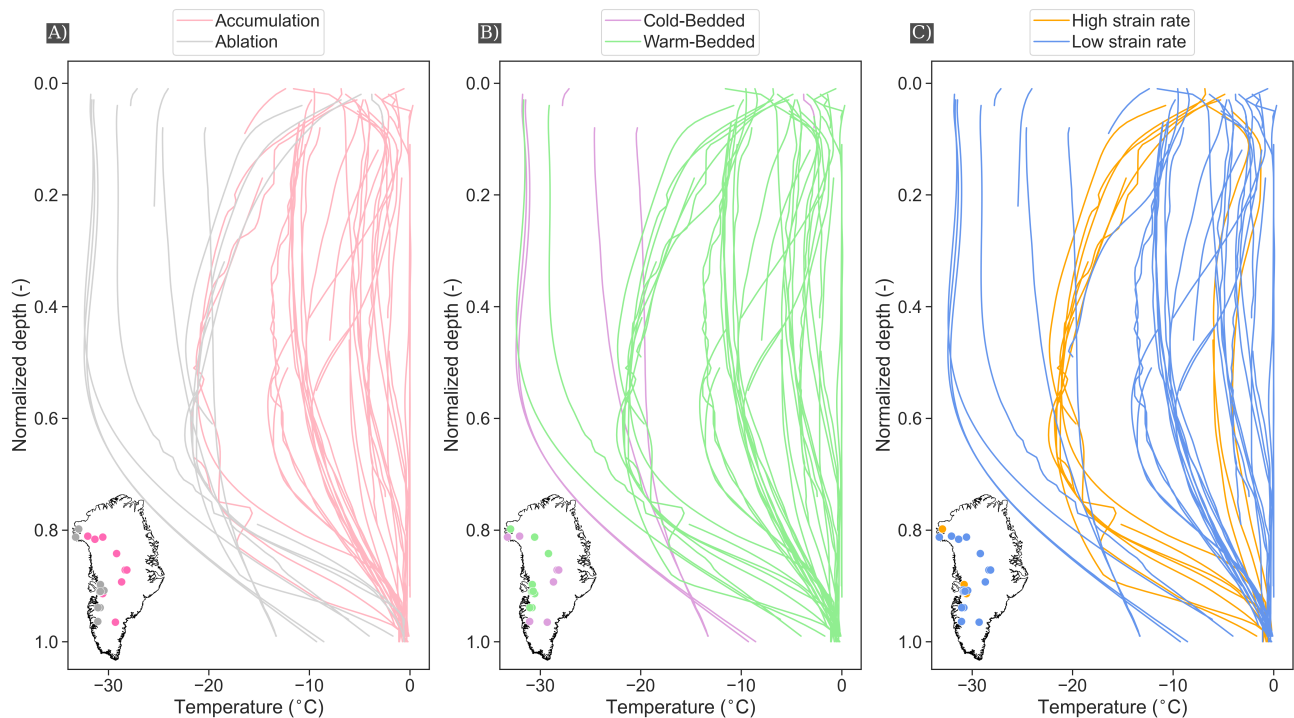
Figure 6. Observed temperature profiles on normalized depth scale for three characteristic regimes. **(A)**: Surface mass balance regime with profiles located in the ablation area (pink) or the accumulation area (gray). **(B)**: Basal thermal state regime with profiles either cold-bedded (purple) or warm-bedded (green). **(C)**: Ice dynamic regime with profiles located either in high-strain rate regions (orange) or low-strain rate regions (blue).

The difference between the modeled and observed profiles was calculated at 0.01 normalized vertical resolution and then aggregated into coarser vertical layers at 0.1 normalized vertical resolution (Figure 7). This method of examining profiles in vertical sections provides better insight on depth-variations of model bias than reducing every profile into a single metric of best fit. This vertical boxplot analysis can also provide some insight on which terms in the energy balance – advection, diffusion, heat production, or latent heat transfer – may be responsible for differences between modeled and the observed profiles, as the relative importance of these terms varies with depth. Where our comparison boxplots show negative temperature differences, modeled temperature values are smaller than observed temperatures, implying that this PISM run is underestimating temperatures. Vice versa where boxplot temperature differences are larger than 0 °C.

The surface mass balance regime comparison generally highlights a better PISM fit to observations in the accumulation area than the ablation zone (Figure 7). This is generally expected, since the accumulation area more closely represents the theoretical steady-state temperature profiles upon which classic ice flow heat equations are predicated. The accumulation boxplot shows that the mean difference value shifts from being positive in the upper part of the profile to negative, with a greater spread in differences, in the bottom 20% of the profile. In comparison, both the ablation and temperate boxplots, which
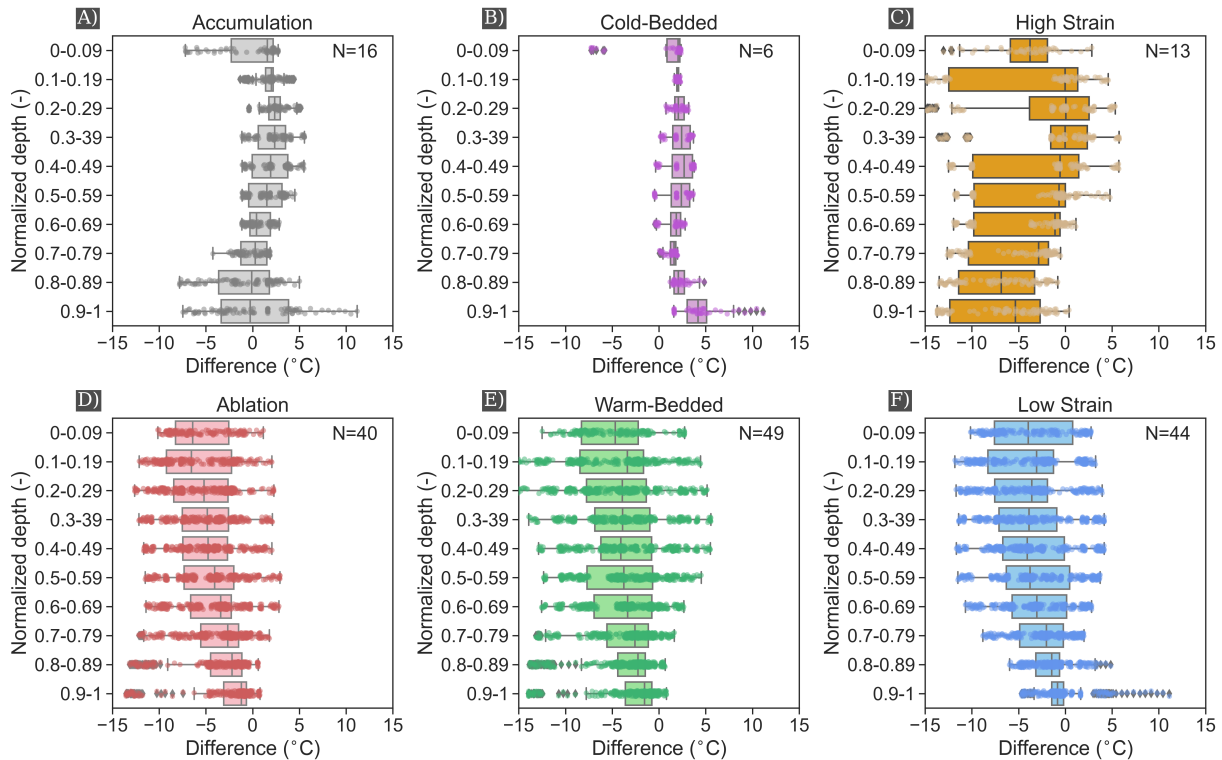
Figure 7. Each plot shows the difference between the modeled minus observed normalized depth profiles aggregated into coarser vertical layers of 0.1 resolution. **(A), (D)**: Surface mass balance regime. **(B), (E)**: Basal thermal state regime. **(C), (F)**: Ice dynamic strain regime. The N value shows the number of profiles the boxplot is based on. Points plotted on top of each boxplot shows individual temperature difference values for all of the profiles at that depth within that category.

share strong overlap in comprising profiles, are clearly less well captured by PISM. These warmer ablation area profiles show a larger spread in difference values throughout the entire vertical profile. Importantly, both boxplots show a systematic negative mean difference at all depths, meaning the simulation consistently underestimates ice temperatures. This may suggest that

305 one or more heat sources are being poorly represented in warmer ablation areas in this particular PISM simulation. This is a general problem for solving the heat equation in all ice flow models. Previous studies similarly showed poor representation of the ablation area and the need to include additional heating sources to reproduce the higher observed englacial temperatures (McDowell et al., 2021).

After excluding profiles where modeled thickness is less than 50 m, the cold-bedded regime boxplot represents the smallest

310 sample size of just five profiles (Camp Century, Dye-3, GISP2, GRIP, and Station Central). These profiles are all drilled at inland locations where the ice is moving relatively slowly. This generally limits the role of horizontal heat advection at these sites. In contrast to the warm-bedded and ablation boxplots, the cold-bedded boxplot shows a systematic positive mean difference over all vertical layers, meaning that modeled temperatures generally overestimate observed temperatures over the

entire column of ice. The largest differences between modeled and observed temperatures (+4 °C on average) however, are found near the ice-sheet bed. Here, where vertical ice advection becomes small, diffusion of geothermal flow should be the most influential term of the heat equation. As heat diffusion is generally well-represented and well-constrained in all ice flow models, this may suggest that this particular PISM simulation employs too high a geothermal heat flow into the ice-sheet base. We note that the geothermal flow is poorly constrained under the Greenland Ice Sheet (Rezvanbehbahani et al., 2017; Colgan et al., 2022) and over long spin-up periods, even small deviations in geothermal heat flow can result in large variations in ice temperature.

The shape of temperature profiles in fast-flowing high-strain regions is expected to have a C-shape associated with strong horizontal advection of upstream ice temperatures (Cuffey and Paterson, 2010; Iken et al., 1993). While this advection of relatively cold upstream ice cools the middle depths of the ice temperature profile, in comparison to the surface boundary condition, deformational heating warms the lower depths (Cuffey and Paterson, 2010). The high strain boxplot shows that the PISM simulation appears to systematically underestimate ice temperatures in the lowermost 50% of the ice sheet. This bias reaches up to -5 °C, on average, between 80-90% depth. This underestimation of ice temperatures near the bed may result from this particular PISM simulation underestimating strain heating associated with enhanced ice deformation in softer Last Glacial Period ice (e.g. Lüthi et al., 2002; Karlsson et al., 2013). Generally, however, it is challenging to simulate temperature profiles in high-strain ice flow regimes, as this requires correct parameterization of both local and upstream heat budgets, as well as the horizontal advection profile linking these heat budgets, in order to correctly represent steep gradients in the ice temperature profile (Cuffey and Paterson, 2010).

The low strain boxplot shows a systematic negative mean difference value across all ice depths. This suggests that, in slow-flowing regions, the model generally underestimates ice temperatures. This might be explained by this particular PISM simulation employing a spin-up surface boundary condition that was either too cold air temperature or too high accumulation rate. As vertical ice advection is dependent on accumulation rate, overestimated accumulation rates can result in overestimated vertical advection rates, which enhance the advection of relatively cold near-surface ice deeper into the ice sheet. The low strain regime profiles are diverse, however, comprising both ablation and accumulation area profiles – and with both cold and warm beds. The low strain regime generally has the largest spread of difference values. This makes it difficult, in comparison to the other boxplots presented here, to interpret a process-level mechanism for the systematic cold bias across these diverse sites.

In this modeled run key parameters influencing the modeled temperatures are the enthalpy, which requires understanding of the liquid water fraction in the ice column and its evolution in time, the geothermal heat flow which also have the potential to affect the presence of water in a given location, and the surface boundary conditions i.e. accumulation rate, which control vertical temperature advection, and ice surface temperatures. These parameters are all very difficult to constrain, however, this is especially the case for the enthalpy and the geothermal heat flow parameter.

7 Outlook

We have compiled 95 ice temperature profiles from 85 individual boreholes from Greenland and the Canadian Arctic into a comprehensive and consistent community resource. This constitutes an increase of +54 ice temperature profiles over what was previously available in open-access data repositories (64% of the database). The scientific community is encouraged to contribute missing or new data or metadata to the database either by contacting the author team or using the GitHub issue pathway. While we expect the primary use of this database to be evaluating simulated 3-D ice temperature fields from thermo-mechanical ice flow models, there may soon be a sufficient number of ice temperature profiles from the Greenland Ice Sheet and peripheral ice caps to use machine learning approaches to spatially interpolate ice temperatures between boreholes on the basis of independent geophysical variables. This database may possibly serve as a modest first step towards addressing this, and other, emerging challenges associated with understanding the thermal state of ice in Greenland and the Canadian Arctic.

We provide an initial comparison between observed ice temperature profiles and those simulated by the PISM ice flow model. This comparison highlights the inherent challenge of comparing 1-D observational datasets with uneven spatial distribution to a simulated 3-D temperature field. These challenges include: the uneven ice thickness between modeled and observed geometry, especially at marginal sites; resolving the difference between the systematic biases and random error in the modeled temperature profiles; and confronting fundamental uncertainty in basal thermal state due to complex processes. In this comparison, the poor representation of cryo-hydrological warming, or the transfer of latent energy, appears to be contributing to a model cold bias at peripheral ice-sheet sites. Similarly, poor representation of deformational heating and vertical ice stratigraphy appears to be contributing to a model cold bias at high-strain rate sites. Clearly, thermo-mechanical models provide the most reliable solution to the heat equation in low-strain, cold-bedded inland areas.

Data availability. The Greenland deep ice temperature database described here is available at https://doi.org/10.22008/FK2/3BVF9V(Mankoff et al., 2022). The source or inputs to the database are available at https://github.com/GEUS-PROMICE/greenland_ice_borehole_temperature_profiles(Last Access 3 March 2022; Mankoff (2022)). The supplementary metadata described in this article, including profile classification is available in the supplementary information of this article.

Users of this product should cite the data repository (Mankoff et al., 2022), and this descriptive data article. Users of this product should also cite the original "Data Source" and "Data DOI" repositories when they are available. We encourage data users to similarly consult relevant "Science Source" articles, which can be found in the metadata for each profile. Furthermore, data users who are generating derivative products from database entries are requested to invite collaboration with the "Science Source" team associated with the database entries being utilized.

Author contributions. Author contribution is captured following the CRediT system. Conceptualization by WC, KM. Data curation by WC, KM, HHT, GDC, DF, CZ, MPL, BV, DDJ, IM, HZ, TM, SHD, AA, B. Hills, RL, JH, NH, B. Hubbard, PC, MJ, JS. Formal analysis by AL, SHD, AA, RL, JH. Funding acquisition by JH, B. Hubbard, PC. Investigation by AL, SHD, AA, RL, JH, B. Hubbard, PC. Interpretation by

AL, AS, HT, GDC, MPL, NBK, HZ, SHD, RL, JH, B. Hubbard, PC. Methodology by AL, KM, WC, GDC, NBK, RL, JH, B. Hubbard, PC. Project administration by KM, WC, RSF, SAK, JH, B. Hubbard, PC. Resources by RSF, SAK. Software by KM. Supervision by KM, WC, JH, B. Hubbard, PC. Validation by AL, KM, WC, AS, NBK, SHD. Visualization by AL, KM. Writing pre-submission by AL, KM, WC, GDC, NBK, HZ, SHD, RL, B. Hubbard, PC.

380 *Competing interests.* The authors declare that they have no conflict of interest.

Acknowledgements. Development of this database by the Geological Survey of Denmark and Greenland (GEUS) was supported by the Programme for Monitoring of the Greenland ice sheet (www.promice.dk), Independent Research Fund Denmark (IRFD) award 8049-00003B, and Villum Foundation award 00022885. Ice coring on Canadian Arctic ice caps was primarily supported by the Polar Continental Shelf Project and the Geological Survey of Canada (Natural Resources Canada), with additional funding from the Canadian Foundation for Climate and Atmospheric Science (Prince of Wales Icefield 2005) and Japan's Science and Technology Agency (Penny ice cap, 1996). Harry
385 Zekollari acknowledges funding from the Fonds de la Recherche Scientifique – FNRS (postdoctoral grant – chargé de recherches) and PROTECT, which has received funding from the European Union's Horizon 2020 research and innovation programme under grant agreement No. 869304. Ice temperature measurements on Store Glacier were supported by the European Union's Horizon 2020 research and innovation programme under grant agreement 683048 (RESPONDER), the National Environment Research Council (NERC) (SAFIRE grants NE/K006126 and NE/K005871/1), and an Aberystwyth University Capital Equipment grant. A. Aschwanden was supported by NASA grant
390 20-CRYO2020-0052. R. Law acknowledges funding from NERC Doctoral Training Partnership studentship grant NE/L002507/1. Mylène Jacquemart acknowledges funding from the Swiss National Science Foundation (grant SNF 184634 PROGGRES). Harper, Humphrey, Meierbachtol, McDowell and Hills funded by the U.S. National Science Foundation, Office of Polar Programs (grant nos. 1203451 and 0909495). G. Clow acknowledges funding from the U.S. Geological Survey and the U.S. National Science Foundation, Office of Polar Programs. Martin
395 P. Lüthi acknowledges funding from the Swiss National Science Foundation, project number 200021_127197. Julien Seguinot acknowledges funding from the Swiss National Science Foundation (SNSF) grants no. 200020-169558 and 200021-153179/1 to Martin Funk (ETHZ), and Trond Mohn Stiftelse (TMS) and University of Bergen (UiB) startup grant 'TMS2022STG03' to Suzette Flantua (UiB).

We also thank Baptiste Vandercrux and Joseph A. MacGregor for their discussion during the development of this database.

References

Aschwanden, A., Bueler, E., Khroulev, C., and Blatter, H.: An enthalpy formulation for glaciers and ice sheets, Journal of Glaciology, 58, 441–457, https://doi.org/10.3189/2012JoG11J088, 2012.

Aschwanden, A., Fahnestock, M. A., and Truffer, M.: Complex Greenland outlet glacier flow captured, Nature communications, 7, 1–8, https://doi.org/10.1038/ncomms10524, 2016.

Aschwanden, A., Fahnestock, M. A., Truffer, M., Brinkerhoff, D. J., Hock, R., Khroulev, C., Mottram, R., and Khan, S. A.: Contribution of the Greenland Ice Sheet to sea level over the next millennium, Science Advances, 5, eaav9396, https://doi.org/10.1126/sciadv.aav9396, 2019.

Aschwanden, A., Bartholomaus, T. C., Brinkerhoff, D. J., and Truffer, M.: Brief communication: A roadmap towards credible projections of ice sheet contribution to sea-level, The Cryosphere Discussions, 2021, 1–14, https://doi.org/10.5194/tc-2021-175, 2021.

Bindschadler, R. A., Nowicki, S., Abe-Ouchi, A., Aschwanden, A., Choi, H., Fastook, J., Granzow, G., Greve, R., Gutowski, G., Herzfeld, U., and et al.: Ice-sheet model sensitivities to environmental forcing and their use in projecting future sea level (the SeaRISE project), Journal of Glaciology, 59, 195–224, https://doi.org/10.3189/2013JoG12J125, 2013.

Blatter, H. and Kappenberger, G.: Mass balance and thermal regime of Laika ice cap, Coburg Island, NWT, Canada, Journal of Glaciology, 34, 102–110, 1988.

Buchardt, S. L. and Dahl-Jensen, D.: Estimating the basal melt rate at NorthGRIP using a Monte Carlo technique, Annals of Glaciology, 45, 137–142, https://doi.org/10.3189/172756407782282435, 2007.

Bueler, E. and Brown, J.: Shallow shelf approximation as a "sliding law" in a thermodynamically coupled ice sheet model, J. Geophys. Res., 114, F03 008, https://doi.org/10.1029/2008JF001179, 2009.

Calov, R. and Hutter, K.: The thermomechanical response of the Greenland Ice Sheet to various climate scenarios, Climate Dynamics, 12, 243–260, https://doi.org/https://doi.org/10.1007/BF00219499, 1996.

Clarke, G. K., Fisher, D. A., and Waddington, E. D.: Wind pumping: a potentially significant heat source in ice sheets, International Association of Hydrological Sciences Publication, 170, 169–180, 1987.

Classen, D.: Temperature profiles for the Barnes Ice Cap surge zone, Journal of Glaciology, 18, 391–405, 1977.

Clow, G. D.: USGS polar temperature logging system, description and measurement uncertainties, Tech. rep., US Department of the Interior, US Geological Survey, https://doi.org/10.3133/tm2E3, 2008.

Clow, G. D.: Temperature data acquired from the DOI/GTN-P Deep Borehole Array on the Arctic Slope of Alaska, 1973–2013, Earth System Science Data, 6, 201–218, https://doi.org/10.5194/essd-6-201-2014, 2014.

Clow, G. D., Saltus, R. W., and Waddington, E. D.: A new high-precision borehole-temperature logging system used at GISP2, Greenland, and Taylor Dome, Antarctica, Journal of Glaciology, 42, 576–584, 1996.

Colbeck, S. and Gow, A.: The margin of the Greenland Ice Sheet at ISUA, Journal of Glaciology, 24, 155–165, 1979.

Colgan, W., Sommers, A., Rajaram, H., Abdalati, W., and Frahm, J.: Considering thermal-viscous collapse of the Greenland Ice Sheet, Earth's future, 3, 252–267, https://doi.org/10.1002/2015EF000301, 2015.

Colgan, W., Wansing, A., Mankoff, K., Lösing, M., Hopper, J., Louden, K., Ebbing, J., Christiansen, F. G., Ingeman-Nielsen, T., Liljedahl, L. C., MacGregor, J. A., Hjartarson, A., Bernstein, S., Karlsson, N. B., Fuchs, S., Hartikainen, J., Liakka, J., Fausto, R. S., Dahl-Jensen, D., Bjørk, A., Naslund, J.-O., Mørk, F., Martos, Y., Balling, N., Funck, T., Kjeldsen, K. K., Petersen, D., Gregersen, U., Dam, G., Nielsen,

435   T., Khan, S. A., and Løkkegaard, A.: Greenland Geothermal Heat Flow Database and Map (Version 1), Earth System Science Data, 14, 2209–2238, https://doi.org/10.5194/essd-14-2209-2022, 2022.

Cuffey, K. M. and Clow, G. D.: Temperature, accumulation, and ice sheet elevation in central Greenland through the last deglacial transition, Journal of Geophysical Research: Oceans, 102, 26 383–26 396, https://doi.org/https://doi.org/10.1029/96JC03981, 1997.

Cuffey, K. M. and Paterson, W. S. B.: The physics of glaciers, Academic Press, 2010.

440   Cuffey, K. M., Clow, G. D., Alley, R. B., Stuiver, M., Waddington, E. D., and Saltus, R. W.: Large arctic temperature change at the Wisconsin-Holocene glacial transition, Science, 270, 455–458, 1995.

Dahl-Jensen, D., Mosegaard, K., Gundestrup, N., Clow, G. D., Johnsen, S. J., Hansen, A. W., and Balling, N.: Past temperatures directly from the Greenland Ice Sheet, Science, 282, 268–271, 1998.

Davis, R.: Approach roads, Greenland 1960-1964., Tech. rep., Cold Regions Research and Engineering Lab Hanover NH, 1967.

445   Doyle, S., Hubbard, B., Christoffersen, P., Young, T. J., Hofstede, C., Bougamont, M., Box, J., and Hubbard, A.: SAFIRE borehole, AWS and GPS datasets (Version 1), figshare, https://doi.org/10.6084/m9.figshare.5745294.v1, 2018a.

Doyle, S. H., Hubbard, B., Christoffersen, P., Young, T. J., Hofstede, C., Bougamont, M., Box, J., and Hubbard, A.: Physical conditions of fast glacier flow: 1. Measurements from boreholes drilled to the bed of Store Glacier, West Greenland, Journal of Geophysical Research: Earth Surface, 123, 324–348, https://doi.org/10.1002/2017JF004529, 2018b.

450   Fischer, H., Werner, M., Wagenbach, D., Schwager, M., Thorsteinnson, T., Wilhelms, F., Kipfstuhl, J., and Sommer, S.: Little ice age clearly recorded in northern Greenland ice cores, Geophysical Research Letters, 25, 1749–1752, https://doi.org/https://doi.org/10.1029/98GL01177, 1998.

Funk, M., Echelmeyer, K., and Iken, A.: Mechanisms of fast flow in Jakobshavns Isbræ, West Greenland: Part II. Modeling of englacial temperatures, Journal of Glaciology, 40, 569–585, 1994.

455   Goelzer, H., Robinson, A., Seroussi, H., and Van De Wal, R. S.: Recent progress in Greenland Ice Sheet modelling, Current climate change reports, 3, 291–302, https://doi.org/10.1007/s40641-017-0073-y, 2017.

Goelzer, H., Nowicki, S., Payne, A., Larour, E., Seroussi, H., Lipscomb, W. H., Gregory, J., Abe-Ouchi, A., Shepherd, A., Simon, E., et al.: The future sea-level contribution of the Greenland Ice Sheet: a multi-model ensemble study of ISMIP6, The Cryosphere, 14, 3071–3096, https://doi.org/10.5194/tc-14-3071-2020, 2020.

460   Gowan, E. J., Zhang, X., Khosravi, S., Rovere, A., Stocchi, P., Hughes, A. L., Gyllencreutz, R., Mangerud, J., Svendsen, J.-I., and Lohmann, G.: A new global ice sheet reconstruction for the past 80 000 years, Nature communications, 12, 1–9, https://doi.org/10.1038/s41467-021-21469-w, 2021.

Gundestrup, N. and Hansen, B. L.: Bore-hole survey at Dye 3, south Greenland, Journal of Glaciology, 30, 282–288, 1984.

Gundestrup, N., Dahl-Jensen, D., Hansen, B., and Kelty, J.: Bore-hole survey at Camp Century, 1989, Cold regions science and technology, 465   21, 187–193, 1993.

Hansen, B. and Landauer, J.: Some results of ice cap drill hole measurements, IASH Publ, 47, 313–317, 1958.

Hansson, M. E.: The Renland ice core. A northern hemisphere record of aerosol composition over 120,000 years, Tellus B: Chemical and Physical Meteorology, 46, 390–418, 1994.

Harper, J.: Ice temperatures measured in a grid of boreholes, Western Greenland, 2014-2016, Arctic Data Center, 470   https://doi.org/doi:10.18739/A24746S04, 2017.

Harper, J. and Meierbachtol, T.: Western Greenland Ice Sheet ice temperature profiles, 2010-2012., Arctic Data Center, https://doi.org/doi:10.18739/A2QV3C51Q, 2021.

Harrington, J. A., Humphrey, N. F., and Harper, J. T.: Temperature distribution and thermal anomalies along a flowline of the Greenland ice sheet, Annals of Glaciology, 56, 98–104, https://doi.org/doi:10.3189/2015AoG70A945, 2015.

475 Heuberger, J. C.: Expéditions Polaires Françaises: Missions Paul-Emil Victor. Glaciologie Groenland Volume 1: Forages sur l'inlandsis, Tech. Rep. 1214, 1954.

Hills, B. H., Harper, J. T., Humphrey, N. F., and Meierbachtol, T. W.: Measured horizontal temperature gradients constrain heat transfer mechanisms in Greenland ice, Geophysical Research Letters, 44, 9778–9785, https://doi.org/10.1002/2017GL074917, 2017.

Hubbard, B., Christoffersen, P., Doyle, S. H., Chudley, T. R., Schoonman, C. M., Law, R., and Bougamont, M.: Borehole-
480 based characterization of ceep mixed-mode crevasses at a Greenlandic outlet glacier, AGU Advances, 2, e2020AV000 291, https://doi.org/10.1029/2020AV000291, e2020AV000291 2020AV000291, 2021a.

Hubbard, B., Christoffersen, P., Doyle, S. H., Chudley, T. R., Schoonman, C. M., Law, R., and Bougamont, M.: Supporting data for 'Borehole-based characterization of deep crevasses at a Greenlandic outlet glacier' published in AGU Advances, figshare, https://doi.org/10.6084/m9.figshare.13400072.v2, 2021b.

485 Humphrey, N. and Echelmeyer, K.: Hot-water drilling and bore-hole closure in cold ice, Journal of Glaciology, 36, 287–298, https://doi.org/10.3189/002214390793701354, 1990.

Huybrechts, P., Letreguilly, A., and Reeh, N.: The Greenland ice sheet and greenhouse warming, Palaeogeography, Palaeoclimatology, Palaeoecology, 89, 399–412, https://doi.org/https://doi.org/10.1016/0031-0182(91)90174-P, 1991.

Iken, A., Echelmeyer, K., Harrison, W., and Funk, M.: Mechanisms of fast flow in Jakobshavns Isbræ, West Greenland: Part I. Measurements
490 of temperature and water level in deep boreholes, Journal of Glaciology, 39, 15–25, https://doi.org/10.3189/S0022143000015689, 1993.

Jezek, K. C., Yardim, C., Johnson, J. T., Macelloni, G., and Brogioni, M.: Analysis of ice-sheet temperature profiles from low-frequency airborne remote sensing, Journal of Glaciology, p. 1–11, https://doi.org/10.1017/jog.2022.19, 2022.

Johnsen, S. J., Dahl-Jensen, D., Dansgaard, W., and Gundestrup, N.: Greenland palaeotemperatures derived from GRIP bore hole temperature and ice core isotope profiles, Tellus B: Chemical and Physical Meteorology, 47, 624–629, https://doi.org/10.3402/tellusb.v47i5.16077,
495 1995.

Karlsson, N. B., Dahl-Jensen, D., Prasad Gogineni, S., and Paden, J. D.: Tracing the depth of the Holocene ice in North Greenland from radio-echo sounding data, Annals of Glaciology, 54, 44–50, https://doi.org/10.3189/2013AoG64A057, 2013.

Karlsson, N. B., Razik, S., Hörhold, M., Winter, A., Steinhage, D., Binder, T., and Eisen, O.: Surface accumulation in Northern Central Greenland during the last 300 years, Annals of Glaciology, 61, 214–224, https://doi.org/10.1017/aog.2020.30, 2020.

500 Kinnard, C., Zdanowicz, C. M., Fisher, D. A., and Wake, C. P.: Calibration of an ice-core glaciochemical (sea-salt) record with sea-ice variability in the Canadian Arctic, Annals of Glaciology, 44, 383–390, https://doi.org/doi:10.3189/172756406781811349, 2006.

Kinnard, C., Koerner, R. M., Zdanowicz, C. M., Fisher, D. A., Zheng, J., Sharp, M. J., Nicholson, L., and Lauriol, B.: Stratigraphic analysis of an ice core from the Prince of Wales Icefield, Ellesmere Island, Arctic Canada, using digital image analysis: High-resolution density, past summer warmth reconstruction, and melt effect on ice core solid conductivity, Journal of Geophysical Research: Atmospheres, 113,
505 https://doi.org/doi:10.1029/2008JD011083, 2008.

Law, R., Christoffersen, P., Hubbard, B., Doyle, S. H., Chudley, T. R., Schoonman, C. M., Bougamont, M., des Tombe, B., Schilperoort, B., Kechavarzi, C., Booth, A., and Young, T. J.: Thermodynamics of a fast-moving Greenlandic outlet glacier revealed by fiber-optic distributed temperature sensing, Science Advances, 7, eabe7136, https://doi.org/10.1126/sciadv.abe7136, 2021.

Lemark, A. and Dahl-Jensen, D.: A study of the Flade Isblink ice cap using a simple ice flow model, Master's thesis, Niels Bohr Institute,
510 Copenhagen University, 2010.

Letréguilly, A., Reeh, N., and Huybrechts, P.: The Greenland ice sheet through the last glacial-interglacial cycle, Palaeogeography, Palaeo-climatology, Palaeoecology, 90, 385–394, https://doi.org/https://doi.org/10.1016/S0031-0182(12)80037-X, 1991.

Lüthi, M., Funk, M., Iken, A., Gogineni, S., and Truffer, M.: Mechanisms of fast flow in Jakobshavn Isbræ, West Greenland: Part III. Measurements of ice deformation, temperature and cross-borehole conductivity in boreholes to the bedrock, Journal of Glaciology, 48, 369–385, https://doi.org/doi:10.3189/172756502781831322, 2002.

Lüthi, M. P., Ryser, C., Andrews, L. C., Catania, G. A., Funk, M., Hawley, R. L., Hoffman, M. J., and Neumann, T. A.: Heat sources within the Greenland Ice Sheet: dissipation, temperate paleo-firn and cryo-hydrologic warming, The Cryosphere, 9, 245–253, https://doi.org/10.5194/tc-9-245-2015, 2015.

Macelloni, G., Leduc-Leballeur, M., Montomoli, F., Brogioni, M., Ritz, C., and Picard, G.: On the retrieval of inter-nal temperature of Antarctica Ice Sheet by using SMOS observations, Remote Sensing of Environment, 233, 111 405, https://doi.org/https://doi.org/10.1016/j.rse.2019.111405, 2019.

MacGregor, J. A., Fahnestock, M. A., Catania, G. A., Aschwanden, A., Clow, G. D., Colgan, W. T., Gogineni, S. P., Morlighem, M., Nowicki, S. M., Paden, J. D., et al.: A synthesis of the basal thermal state of the Greenland Ice Sheet, Journal of Geophysical Research: Earth Surface, 121, 1328–1350, https://doi.org/10.1002/2015JF003803, 2016.

MacGregor, J. A., Fahnestock, M. A., Colgan, W. T., Larsen, N. K., Kjeldsen, K. K., and Welker, J. M.: The age of surface-exposed ice along the northern margin of the Greenland Ice Sheet, Journal of Glaciology, 66, 667–684, https://doi.org/10.1017/jog.2020.62, 2020.

Machguth, H., Thomsen, H. H., Weidick, A., Ahlstrøm, A. P., Abermann, J., Andersen, M. L., Andersen, S. B., Bjørk, A. A., Box, J. E., Braithwaite, R. J., et al.: Greenland surface mass-balance observations from the ice-sheet ablation area and local glaciers, Journal of Glaciology, 62, 861–887, https://doi.org/10.1017/jog.2016.75, 2016.

Maguire, R., Schmerr, N., Pettit, E., Riverman, K., Gardner, C., DellaGiustina, D. N., Avenson, B., Wagner, N., Marusiak, A. G., Habib, N., Broadbeck, J. I., Bray, V. J., and Bailey, S. H.: Geophysical constraints on the properties of a subglacial lake in northwest Greenland, The Cryosphere, 15, 3279–3291, https://doi.org/10.5194/tc-15-3279-2021, 2021.

Mankoff, K. D.: Greenland deep ice temperature database, github, https://github.com/GEUS-Glaciology-and-Climate/greenland_ice_borehole_temperature_profiles, 2022.

Mankoff, K. D., Løkkegaard, A., Thomsen, H., Clow, G., Fisher, D., Zdanowicz, C., Lüthi, M. P., Vinther, B., MacGregor, J. A., McDowell, I., Zekollari, H., Meierbachtol, T., Doyle, S., Law, R., Hills, B., Harper, J., Humphrey, N., Hubbard, B., Christof-fersen, P., Jacquemart, M., Julien, S., and Colgan, W.: Greenland and Canadian Arctic ice temperature profiles database, dataverse, https://doi.org/10.22008/FK2/3BVF9V, 2022.

McDowell, I. E., Humphrey, N. F., Harper, J. T., and Meierbachtol, T. W.: The cooling signature of basal crevasses in a hard-bedded region of the Greenland Ice Sheet, The Cryosphere, 15, 897–907, https://doi.org/10.5194/tc-15-897-2021, 2021.

Meierbachtol, T. W., Harper, J. T., Johnson, J. V., Humphrey, N. F., and Brinkerhoff, D. J.: Thermal boundary conditions on western Green-land: Observational constraints and impacts on the modeled thermomechanical state, Journal of Geophysical Research: Earth Surface, 120, 623–636, https://doi.org/10.1002/2014JF003375, 2015.

Moon, T., Fisher, M., Harden, L., and Stafford, T.: QGreenland (v1. 0.1), software]. Available from https://qgreenland. org. https://doi. org/10.5281/zenodo, 4558266, https://doi.org/10.5281/zenodo.4558266, 2021.

Morlighem, M., Williams, C. N., Rignot, E., An, L., Arndt, J. E., Bamber, J. L., Catania, G., Chauché, N., Dowdeswell, J. A., Dorschel, B., Fenty, I., Hogan, K., Howat, I., Hubbard, A., Jakobsson, M., Jordan, T. M., Kjeldsen, K. K., Millan, R., Mayer, L., Mouginot, J., Noël, B. P. Y., O'Cofaigh, C., Palmer, S., Rysgaard, S., Seroussi, H., Siegert, M. J., Slabon, P., Straneo, F., van den Broeke,

M. R., Weinrebe, W., Wood, M., and Zinglersen, K. B.: BedMachine v3: Complete bed topography and ocean bathymetry mapping of Greenland from multibeam echo sounding combined with mass conservation, Geophysical Research Letters, 44, 11,051–11,061, https://doi.org/10.1002/2017GL074954, 2017.

Muto, A., Scambos, T. A., Steffen, K., Slater, A. G., and Clow, G. D.: Recent surface temperature trends in the interior of East Antarctica from borehole firn temperature measurements and geophysical inverse methods, Geophysical Research Letters, 38, https://doi.org/https://doi.org/10.1029/2011GL048086, 2011.

Paterson, W.: A temperature profile through the Meighen ice cap, Arctic Canada, International Association of Scientific Hydrology, Publication, 79, 440–449, 1968.

Paterson, W., Koerner, R., Fisher, D., Johnsen, S., Clausen, H., Dansgaard, W., Bucher, P., and Oeschger, H.: An oxygen-isotope climatic record from the Devon Island ice cap, arctic Canada, Nature, 266, 508–511, 1977.

Phillips, T., Rajaram, H., Colgan, W., Steffen, K., and Abdalati, W.: Evaluation of cryo-hydrologic warming as an explanation for increased ice velocities in the wet snow zone, Sermeq Avannarleq, West Greenland, Journal of Geophysical Research: Earth Surface, 118, 1241–1256, https://doi.org/10.1002/jgrf.20079, 2013.

Rasmussen, S. O., Abbott, P. M., Blunier, T., Bourne, A. J., Brook, E., Buchardt, S. L., Buizert, C., Chappellaz, J., Clausen, H. B., Cook, E., Dahl-Jensen, D., Davies, S. M., Guillevic, M., Kipfstuhl, S., Laepple, T., Seierstad, I. K., Severinghaus, J. P., Steffensen, J. P., Stowasser, C., Svensson, A., Vallelonga, P., Vinther, B. M., Wilhelms, F., and Winstrup, M.: A first chronology for the North Greenland Eemian Ice Drilling (NEEM) ice core, Climate of the Past, 9, 2713–2730, https://doi.org/10.5194/cp-9-2713-2013, 2013.

Rezvanbehbahani, S., Stearns, L. A., Kadivar, A., Walker, J. D., and van der Veen, C. J.: Predicting the Geothermal Heat Flux in Greenland: A Machine Learning Approach, Geophysical Research Letters, 44, 12,271–12,279, https://doi.org/10.1002/2017GL075661, 2017.

Rohatgi, A.: Webplotdigitizer: Version 4.5, https://automeris.io/WebPlotDigitizer, 2021.

Ryser, C., Lüthi, M. P., Andrews, L. C., Hoffman, M. J., Catania, G. A., Hawley, R. L., Neumann, T. A., and Kristensen, S. S.: Sustained high basal motion of the Greenland ice sheet revealed by borehole deformation, Journal of Glaciology, 60, 647–660, https://doi.org/10.3189/2014JoG13J196, 2014.

Seguinot, J., Funk, M., Bauder, A., Wyder, T., Senn, C., and Sugiyama, S.: Englacial warming indicates deep crevassing in Bowdoin glacier, Greenland, Frontiers in Earth Science, 8, 65, https://doi.org/10.3389/feart.2020.00065, 2020.

Shapiro, N. M. and Ritzwoller, M. H.: Inferring surface heat flux distributions guided by a global seismic model: particular application to Antarctica, Earth and Planetary Science Letters, 223, 213–224, https://doi.org/10.1016/j.epsl.2004.04.011, 2004.

Stauffer, B. and Oeschger, H.: Temperaturprofile in Bohrlöchern am Rande des grönländischen Inlandeises, Eidg. Tech. Hochschule, Zurich Versuchsanst. Wasserbau, Hydrol. Glaziol. Mill, 41, 301–313, 1979.

Tarasov, L. and Peltier, W.: A geophysically constrained large ensemble analysis of the deglacial history of the North American ice-sheet complex, Quaternary Science Reviews, 23, 359–388, https://doi.org/doi.org/10.1016/j.quascirev.2003.08.004, 2004.

Thomsen, H., Olesen, O. B., Braithwaite, R. J., and Bøggild, C. E.: Ice drilling and mass balance at Pâkitsoq, Jakobshavn, central West Greenland, Rapport Grønlands Geologiske Undersøgelse, 152, 80–84, https://doi.org/10.34194/rapggu.v152.8160, 1991.

Thomsen, H. H., Reeh, N., Olesen, O. B., and Jonsson, P.: Glacier and climate research on Hans Tausen Iskappe, North Greenland–1995 glacier basin activities and preliminary results, Bulletin Grønlands Geologiske Undersøgelse, 172, 78–84, 1996.

Wohlleben, T., Sharp, M., and Bush, A.: Factors influencing the basal temperatures of a High Arctic polythermal glacier, Annals of Glaciology, 50, 9–16, https://doi.org/10.3189/172756409789624210, 2009.

Zagorodnov, V., Nagornov, O., Scambos, T., Muto, A., Mosley-Thompson, E., Pettit, E., and Tyuflin, S.: Borehole temperatures reveal details of 20th century warming at Bruce Plateau, Antarctic Peninsula, The Cryosphere, 6, 675–686, https://doi.org/10.5194/tc-6-675-2012, 2012.

Zekollari, H., Huybrechts, P., Noël, B., van de Berg, W. J., and van den Broeke, M. R.: Sensitivity, stability and future evolution of the world's northernmost ice cap, Hans Tausen Iskappe (Greenland), The Cryosphere, 11, 805–825, https://doi.org/10.5194/tc-11-805-2017, 2017.